

1 **The mycotoxin alternariol induces DNA damage and modify**  
2 **macrophage phenotype and inflammatory responses**

3 A. Solhaug<sup>1\*</sup>, C. Wisbech<sup>1</sup>, T.E. Christoffersen<sup>2,3</sup>, L.O. Hult<sup>3,4</sup>, T. Lea<sup>3</sup>, G.S. Eriksen<sup>1</sup> and J.A.  
4 Holme<sup>5</sup>.

5  
6 <sup>1</sup>Norwegian Veterinary Institute, 0454 Oslo, Norway, <sup>2</sup>Faculty of Engineering, Ostfold University College,  
7 1757 Halden, Norway, <sup>3</sup>Department of Chemistry, Biotechnology and Food Science, Norwegian  
8 University of Life Sciences, Aas, Norway, <sup>4</sup>Ostfold Hospital Trust, 1603 Fredrikstad, Norway, <sup>5</sup>Division of  
9 Environmental medicine, Norwegian Institute of public health, 0379 Oslo, Norway

10

11

12

13

14

15

16 \*Corresponding author:

17 Anita Solhaug, PhD

18 Norwegian Veterinary Institute,

19 P.O.BOX 750 Sentrum, 0106 Oslo, Norway

20

21 Tel: +47 23216214; Fax: +47 23216201

22 E-mail: [Anita.Solhaug@vetinst.no](mailto:Anita.Solhaug@vetinst.no)

23 **Abstract**

24 Alternariol (AOH), a mycotoxin produced by *Alternaria* fungi, is frequently found as a  
25 contaminant in fruit and grain products. Here we examined if AOH could modify macrophage  
26 phenotype and inflammatory responses. In RAW 264.7 mouse macrophages AOH changed the  
27 cell morphology of from round to star-shaped cells, with increased levels of CD83, CD86,  
28 CD11b, MHCII and endocytic activity. TNF $\alpha$  and IL-6 were enhanced at mRNA-level, but only  
29 TNF $\alpha$  showed increased secretion. No changes were found in IL-10 or IL-12p40 expression.  
30 Primary human macrophages changed the cell morphology from round into elongated shapes  
31 with dendrite-like protrusions in response to AOH. The levels of CD83 and CD86 were  
32 increased, HLA-DR and CD68 were down-regulated and CD80, CD200R and CD163 remained  
33 unchanged. Increased secretion of TNF $\alpha$  and IL-6 were found after AOH exposure, while IL-8,  
34 IL-10 and IL-12p70 were not changed. Furthermore, AOH reduced macrophage endocytic  
35 activity and autophagosomes. AOH was also found to induce DNA damage, which is suggested  
36 to be linked to the morphological and phenotypical changes. Thus, AOH was found to change the  
37 morphology and phenotype of the two cell models, but either of them could be characterized as  
38 typical M1/M2 macrophages or as dendritic cells (DC).

39

40 **Keywords:**

41 Macrophages, differentiation, DNA damage, mycotoxins, alternariol

42

43

44

45 **Abbreviations:**

46 AOH, alternariol; AF, autofluorescence; Arg-1, arginase-1; BSA, bovine serum albumin; CBA,  
47 cytometric bead array; CD, cluster of differentiation; DC, dendritic cells; DSBs, DNA double  
48 stranded breaks; ELISA, enzyme-linked immunosorbent assay; GM-CSF, granulocyte  
49 macrophage colony-stimulating factor; iNOS, Inducible nitric oxide synthase; IFN- $\gamma$ , interferon-  
50  $\gamma$ ; IL-4, interleukin-4; IL-10, interleukin-10; IC, Isotype controls; SEM, scanning electron  
51 microscopy; SSBs, DNA single stranded breaks; MFI, median fluorescence intensity; NAC, N-  
52 acetyl-L-cysteine; PBMC, peripheral blood mononuclear cells; PBS, phosphate buffered saline;  
53 PI, propidium iodide; ROS, reactive oxygen species

54

55

56

57

58

## 59 **1. Introduction**

60 Mycotoxins are secondary metabolites produced by fungi that may contaminate all stages of the  
61 food chain. Consumption of mycotoxins is considered an important risk factor for both human  
62 and animal health (Wu *et al.*, 2014). The immune system is considered to be the most sensitive  
63 target for several mycotoxins, including the trichothecenes; with low doses of toxins having  
64 immune-stimulatory effects and higher doses causing immunosuppression (Pestka, 2010). The  
65 mycotoxin alternariol (AOH) is produced by the *Alternaria* fungi, which is ubiquitous in the  
66 environment. *Alternaria* seems to have a great ability to adapt to the environmental conditions  
67 and is therefore found in both humid and semi-dry regions (EFSA, 2011). Toxin production may  
68 also occur at lower temperatures, so food refrigerated during transportation and storage may also  
69 be contaminated (EFSA, 2011). Alternariol is often found in fruit and in processed fruit  
70 products such as juices and wine (Ackermann *et al.*, 2011), as well as in vegetables and grain  
71 (Ostry, 2008; Uhlig *et al.*, 2013). AOH has been found in 31% of samples of feed and agricultural  
72 commodities in Europe (n=300), with concentrations ranging from 6.3 – 1840 mg/kg (EFSA,  
73 2011). The highest levels of AOH are found in legume, nuts and oilseed food (EFSA, 2011). At  
74 present, there are no regulations of AOH in food and feed (EFSA, 2011). Although the human  
75 dietary exposure is estimated to be low (1.9 - 39 ng/kg/bw/day), it exceeds the threshold of  
76 toxicological concern for potential genotoxic compounds (2.5 ng/kg/bw/day) (EFSA, 2011).  
77 Several *in vitro* studies have reported that AOH shows genotoxic effects by the induction of DNA  
78 damage, including single-stranded DNA breaks (SSBs)- and double-stranded DNA breaks  
79 (DSBs) (Pfeiffer *et al.*, 2007; Fehr *et al.*, 2009). A recent *in vivo* study reported that AOH was  
80 negative in the bone marrow micronuclei test and comet assay using liver tissue (Schuchardt *et*  
81 *al.*, 2014). The target organ is, however, most likely the gastrointestinal tract with associated  
82 immune cells and corresponding microbiota (Maresca and Fantini, 2010). Thus, although  
83 negative in the study of Schuchardt and co-workers, possible genotoxic effect of AOH *in vivo* can  
84 still not totally be excluded. The DNA damaging properties found *in vitro* has been suggested to  
85 be due the ability of AOH to act as a topoisomerase poison (Fehr *et al.*, 2009). DNA  
86 topoisomerases are enzymes that regulate the DNA topology during transcription, replication,  
87 chromosome condensation and the maintenance of genome stability (Vos *et al.*, 2011). Our recent  
88 studies using the RAW 264.7 macrophage cell line (Solhaug *et al.*, 2012, 2013, 2014), showed  
89 that exposure to AOH increased the production of reactive oxygen species (ROS) and the level of

90 DNA damage (SSBs, DSBs and oxidative DNA damage). Cells accumulated in G<sub>2</sub>-phase (4N),  
91 with diploid or abnormal partly divided nuclei. Furthermore, the AOH-induced cell cycle arrest  
92 was accompanied by increased autophagy and senescence, which were suggested to be a  
93 consequence of DSBs.

94  
95 Macrophages play a key role in innate and adaptive immunity. Their main function is to perform  
96 phagocytic clearance of pathogens and dying cells and to modulate the adaptive immune response  
97 through antigen processing and presentation and by cytokine secretion. Both tissue-resident  
98 macrophages and monocyte-derived macrophages are recruited during inflammation (Hume *et al.*,  
99 *et al.*, 2008; Mowat and Bain, 2010). Monocytes develop into various forms of macrophages  
100 according to the nature of environmental signals (Hume, 2008; Bain and Mowat, 2014). The main  
101 macrophage polarization states are referred to as classically activated macrophages (M1) and  
102 alternatively activated macrophages (M2), thus mirroring the Th1/Th2 differentiation paradigm  
103 (Biswas *et al.*, 2012; Martinez and Gordon, 2014). Th1-related cytokines such as interferon- $\gamma$   
104 (INF- $\gamma$ ), as well as microbial stimuli such as lipopolysaccharide (LPS) polarize macrophages to  
105 an M1 phenotype. These cells produce pro-inflammatory cytokines such as TNF $\alpha$ , IL-12/23 and  
106 IL-8; and have inducible nitric oxide synthase (iNOS). They are able to ingest (endocytic  
107 activity) and kill pathogens rapidly; however, the use of ROS and NO will also result in tissue  
108 damage (Laskin *et al.*, 2011; Biswas *et al.*, 2012; Mills and Ley, 2014). M1 macrophages have  
109 increased antigen presenting capacity and display increased levels of major histocompatibility  
110 complex class II (MHCII) and B7 co-stimulatory molecules such as CD80 and CD86 (Ambarus  
111 *et al.*, 2012; Biswas *et al.*, 2012). The integrin CD11b is considered being a pan-macrophage  
112 marker, associated with adherence and phagocytosis. M2 polarization is broader and includes IL-  
113 4/IL-13 stimulated macrophages (M2a), IL-10 induced macrophages (M2c) and immune  
114 complex-triggered macrophages (M2b) (Mantovani *et al.*, 2004). M2 macrophages produce anti-  
115 inflammatory cytokines such as IL-10, and are generally involved in tissue regeneration  
116 (Mantovani *et al.*, 2004; Biswas *et al.*, 2012). Typical surface receptors expressed by M2 cells are  
117 the membrane glycoprotein CD200r, which is expressed on M2a cells and the scavenger receptor  
118 CD163, which is expressed on M2c cells (Koning *et al.*, 2010; Ambarus *et al.*, 2012).  
119 Interestingly, proliferation of M2 macrophages rather than recruitment from the blood has  
120 recently been suggested to be important for Th2 responses (Jenkins *et al.*, 2011). Other important

121 markers may include arginase-1 (Arg-1) (Mills and Ley, 2014). Monocytes may also differentiate  
122 into dendritic cells (DC), which are professional antigen-presenting cells (APCs) bridging the  
123 innate and adaptive immune system through activation and expansion of T cells (Coombes and  
124 Powrie, 2008). Immature DCs are located in peripheral tissues to continuously monitor the  
125 environment through the uptake of particulate and soluble products, thus have increased  
126 endocytic and phagocytic activity. Antigen-loaded DCs acquire a mature phenotype, associated  
127 with reduced endocytic and phagocytic capacities, and enhanced production of pro-inflammatory  
128 cytokines (IL-12p70, TNF $\alpha$ , IL-6 and IL-23). The mature DCs, then, migrate towards the  
129 lymphoid organs where they interact with, and activate, naive T cells. In addition to the cytokine  
130 profile, mature DCs are often characterized by increased expression of co-stimulatory molecules  
131 (e.g. CD80, CD86), MHCII, HLA-DR as well as CD83, a conserved marker for mature DC  
132 (Jensen and Gad, 2010, Zhou and Tedder, 1996).

133  
134 Immune cells are potential targets for the adverse health effects of mycotoxins. An optimal  
135 immune response depends on the delicate balance between M1, M2 and DC. We have therefore  
136 investigated the potential effect of AOH on macrophage phenotypes and inflammatory responses.  
137 In our previous studies, the RAW 264.7 macrophage cell line has proven to be a good model for  
138 AOH toxicity (Solhaug *et al.*, 2012, 2013, 2014). To further enhance the relevance for human  
139 risk evaluation, we have extended our studies to also include macrophages derived from human  
140 primary blood monocytes.

141

## 142 **2. Materials and Methods**

143

### 144 **2.1. Reagents and chemicals**

145 Dulbecco's Modified Eagle Medium (DMEM), penicillin/streptomycin and fetal bovine serum  
146 (FBS) were purchased from Lonza (Verviers, Belgium). FITC-dextran (42 kDa), Hoechst 33342,  
147 LPS and collagen were from Sigma-Aldrich (St. Louis, MO, USA). OneComp beads were from  
148 eBioscience. BD OptEIA mouse TNF ELISA kit, BD OptEIA mouse IL-6 ELISA kit and Human  
149 inflammatory bead assay CBA was from BD Biosciences (San Diego, CA, USA). Interleukin 4  
150 (IL-4), Interleukin 10 (IL-10), interferon- $\gamma$  (INF $\gamma$ ) and granulocyte macrophage colony-  
151 stimulating factor (GM-CSF) were from ImmunoTools (Germany). Millicell EZ slides and

152 Mowiol were from Millipore (Hayward, CA, USA) and Upcell plates were purchased from Nunc  
153 (Rochester, NY, USA). H<sub>2</sub>DCFDA-CM, DHE, N-acetyl-L-cysteine (NAC), propidium iodide,  
154 Hoechst and RNase were from, Life technologies (Grand Island, NY, USA).

155 *Antibodies:* Anti-human CD163 Alexa Fluor 647, Alexa Fluor 488 Mouse IgG2b ( $\kappa$  Isotype Ctrl),  
156 anti-human CD83 PE, anti-human CD86 PerCP/Cy5.5, anti-human CD80 Alexa Fluor 488, anti-  
157 human CD200r PE, anti-human CD68 Alexa Fluor 488, anti-mouse CD83 PE, Rat igG1 PE,  
158 human TruStain FcX (Fc Receptor Blocking Solution) and TruStain fcX anti-mouse CD16/32  
159 (mouse Fc receptors blocker), were from BioLegend (San Diego, CA, USA). anti-human HLA-  
160 DR Alexa Fluor 674 were from Bioss (Woburn, MA, USA), anti-mouse CD80 FITC, Armenian  
161 Hamster igG FITC isotype Ctrl, anti-mouse MHCII FITC, Rat igG2b FITC isotype Ctrl, anti-  
162 mouse CD11b Alexa Fluor 488, Rat IgG2b Alexa Fluor 488 isotype Ctrl, anti-mouse CD86 APC  
163 and Rat IgG2ak Iso Control APC were from eBioscience (San Diego, CA, USA).  $\gamma$ H2AX and  
164 LC3B were from cell signaling (Beverly, MA, USA) and anti-rabbit Alexa Fluor 647 were from  
165 molecular probes (Life Technology, Grand Island, NY, USA).

166

## 167 **2.2. Cell cultures**

168 *RAW 264.7 macrophages:* The mouse macrophage cell line RAW 264.7 was obtained from  
169 European Collection of Cell Cultures (ECACC) and grown in DMEM supplemented with 10%  
170 heat inactivated fetal bovine serum (FBS; EU standard, Lonza), penicillin (100 U/ml), and  
171 streptomycin (100  $\mu$ g/ml). The cells were cultured at 37 °C with 5% CO<sub>2</sub> in a humidified  
172 atmosphere and kept in logarithmic growth phase at  $1 \times 10^6$  -  $10 \times 10^6$  cells/75 cm<sup>2</sup> through  
173 routine sub-culturing by scraping, according to standard ECACC protocol. Cells were plated ( $0.3$   
174  $\times 10^6$  cells/cm<sup>2</sup>) 24 h prior to the experiment, which resulted in approximately 70% confluence at  
175 the day of exposure. Medium were refreshed before exposures. For measurement of cell surface  
176 receptors, endocytosis and apoptosis/necrosis, the cells were grown on temperature-responsive  
177 UpCell plates (Nunc, Rochester, NY, USA) from which cells detach at temperatures below 32 °C.  
178 Otherwise the cells were harvested by scraping, as recommended by ECACC.

179 *Primary human macrophages:* Peripheral blood mononuclear cells (PBMCs) were isolated from  
180 buffy coats obtained from healthy donors according to the international ethical guidelines  
181 (CIOMS) (Østfold Hospital Trust, Norway) by Ficoll density gradient centrifugation. About 10%  
182 of the PBMC isolated from human blood is monocytes (Auffray *et al.*, 2009). The PBMCs were

183 cultivated in RPMI 1640 supplemented with 10% heat inactivated FBS and penicillin (100  
184 U/ml)/streptomycin (100 µg/ml), at 37 °C under 5% CO<sub>2</sub>, and plated at a density of 1.0 x  
185 10<sup>6</sup> cells/cm<sup>2</sup>. The PBMCs were cultivated for 24 h to allow the monocytes to adhere to the  
186 plastic. The non-adherent PBMC were washed off with PBS and the monocytes were allowed to  
187 differentiate into macrophages in the presence of granulocyte macrophage colony-stimulating  
188 factor (GM-CSF, 50 ng/ml) for 7 days. The cells were approximately 70% confluent at the day of  
189 exposure. The medium was replenished on day four and on the day of exposure. Cells from  
190 different donors were used for the biological replicates of the experiments. Macrophage purity  
191 and differentiation were verified by flow cytometric analysis of CD68 (Supplementary, Fig. S1).  
192 Positive controls for M1 and M2 differentiation were generated by treatment with GM-CSF (50  
193 ng/ml) alone for the first 4 days, then INF-γ (50 ng/ml) and IL-10 (50 ng/ml) were added,  
194 respectively. For the generation of DCs, the cells were stimulated with GM-CSF (50 ng/ml) + IL-  
195 4 (25 ng/ml) for 6 days and LPS (100 ng/ml) were added and the cell incubated further for 24 h.  
196 The supplemented RPMI 1640 media was exchanged on day four and six. Cell differentiation  
197 was verified by flow cytometric analysis of specific markers associated with the cell type as M1  
198 express CD80, M2 express CD163 and CD200r and DCs express CD83 and DC86 (data not  
199 shown). The cells were harvested by trypsination.

200 *Primary mouse peritoneal macrophages:* Female B6C3F1 mice (5 weeks old) weighing 16 to 18  
201 g were obtained from Charles River Laboratories, Inc (Wilmington, MA, USA) or Harlan  
202 (Indianapolis, IN, USA). Housing, handling and sample collection procedures conformed to the  
203 policies of the Michigan State University All-University Committee on Animal Use and Care in  
204 accordance with NIH guidelines. Mice were injected ip with 1.5 ml of sterile 3% (w/v)  
205 thioglycollate broth. After 4 days, mice were euthanized and macrophages collected by peritoneal  
206 lavage with ice-cold Hank's BSS (Invitrogen Corporation, Carlsbad, CA, USA). Cells were  
207 pelleted by centrifugation at 1100 g for 5 min. Cells were washed with PBS once and re-  
208 suspended in RPMI-1640 containing 10% (v/v) heat-inactivated FBS, penicillin (100 U/ml)/  
209 streptomycin (100 µg/ml) and cultivated cultured at 37 °C under 5% CO<sub>2</sub> in a humidified  
210 incubator (0.4 x 10<sup>6</sup> cells/cm<sup>2</sup>). After 3 h incubation, non-adherent cells were removed. The cells  
211 were then cultivated further for 24 h before treatment. The cells were approximately 70%  
212 confluent at the day of exposure. The cells were harvested by trypsination.

213 *Exposure:* AOH was dissolved in DMSO and the final concentration of solvent in cell culture  
214 was 0.1%. Appropriate controls containing the same amount of solvent were included in each  
215 experiment. For experiments with the antioxidant N-acetyl-L-cysteine (NAC); NAC was  
216 dissolved in complete medium complemented with HEPES (25 mM) and pH adjusted to 7.2. The  
217 cells were pre-treated with NAC for 1 h before exposure to AOH.

218

219

### 220 **2.3. Evaluation of cell morphology**

#### 221 *Fluorescence microscopy:*

222 The cells were seeded and cultivated on Millicell EZ slides. After exposure to AOH, the cells  
223 were fixed in 4% PFA for 10 min at ambient temperature followed by permeabilization and  
224 blocking in 3% BSA/PBS, 0.05% saponin for 1 h. The cells were then stained with Phalloidin  
225 Alexa Fluor 555, diluted in 3% BSA / PBS / 0.05% saponin for 1 h, and washed 3 times for 5 min  
226 with 3% BSA / PBS / 0.05% saponin. The nuclei were stained with Hoechst 33342 (1 $\mu$ g/ $\mu$ l) and  
227 coverslips mounted with mowiol. Pictures were captured with a fluorescence microscope (Nikon  
228 Eclipse 80i, equipped with a DS-Ri1 camera, Amsterdam, Netherlands).

#### 229 *Scanning electron microscopy (SEM):*

230 SEM was done as previously described (Christoffersen *et al.*, 2015). Samples were washed and  
231 fixed with 5% glutaraldehyde in 0.1 M sodium cacodylate and 0.1 M sucrose (pH 7.4) for 45  
232 min; then replaced with 0.1 M sodium cacodylate and 0.1 M sucrose (pH 7.4) for 30 min.  
233 Samples were then washed, dehydrated in graded ethanol series and dried using a critical-point  
234 dryer (CDP 030, BAL-TEC GmbH, Germany). Dry samples were mounted on aluminum stubs  
235 using double-faced carbon tape (Agar Scientific, UK), and coated with approximately 500 Å  
236 platinum using a sputter coater (Polaron SC7640, Quorum Technologies, UK). Microscopic  
237 analyses were performed using an EVO-50 Zeiss microscope (Carl Zeiss AG, Germany).

#### 238 *Light microscopy:*

239 Cell morphology was evaluated by light microscopy (Leica DMIL. Solms, Germany). Random  
240 pictures were taken by Moticam 1000 (Motic, Hong Kong, China).

241

### 242 **2.4. Analysis of phenotypic cell markers by flow cytometry**

243 *RAW 264.7 macrophages*: Following AOH exposure the cells were collected and incubated with  
244 Fc-blocker 30 min on ice. The samples were then stained with direct-conjugated antibodies  
245 toward CD86 APC, CD80 FITC, MHCII FITC, CD11b Alexa Fluor 488 or CD83 PE, or with  
246 their associated isotype controls (at respectively equal concentrations) for 30 min on ice in the  
247 dark. The cells were then washed with 0.5% BSA-PBS twice, re-suspended in PBS and analyzed  
248 by flow cytometry (Accuri C6, BD Biosciences, San Jose, CA, USA). Alexa Fluor 488 or FITC  
249 were detected by using 488<sub>ex</sub>:530/30<sub>em</sub>, PE: 488<sub>ex</sub>:585/42<sub>em</sub>, APC: 647<sub>ex</sub>:675/25<sub>em</sub>. Live (non-  
250 fixated) AOH treated RAW 264.7 cells generated some autofluorescence (AF) compared to  
251 untreated cells. The AF was calculated by using isotype controls (IC) and median fluorescence  
252 intensity (MFI) measurements and subtracted from the MFI of AOH treated cells: AF = MFI (IC  
253 AOH treated cells) – MFI (IC Ctrl cells).

254 *Primary human macrophages*: The cells were collected following exposure and washed twice  
255 with 0.5% BSA in PBS (500xg for 10 min). The cells were re-suspended in 50 µl 0.5% BSA in  
256 PBS, 2.5 µl fc-blocker was added and the cells incubated for 30 min on ice. The directly  
257 conjugated antibodies (CD163 Alexa Fluor 647), CD83 PE, CD86 PerCP/Cy5.5), CD80 Alexa  
258 Fluor 488, CD200r PE, HLA-DR Alexa Fluor 647) were added directly to the cells in the  
259 blocking solution and incubated further on ice in the dark for 30 min. Cells were then washed  
260 twice with 0.5% BSA-PBS, re-suspended in PBS and analyzed by flow cytometry (Accuri C6).  
261 Alexa Fluor 488 was detected by using 488<sub>ex</sub>:530/30<sub>em</sub>, PE: 488<sub>ex</sub>:585/42<sub>em</sub>, PerCP/Cy5.5:  
262 488<sub>ex</sub>:LP670<sub>em</sub>, Alexa Fluor 647: 647<sub>ex</sub>:675/25<sub>em</sub>. AOH treatment did not induce any AF in  
263 human macrophages. As CD68 is an intracellular marker, cells were permeabilized prior to  
264 staining according to manufacturer's guidelines (BioLegend). Cells were stained with CD68  
265 Alexa Fluor 488 or the corresponding isotype control (at equal concentration), as described above  
266 followed by flow cytometric analysis.

267

## 268 **2.5. Endocytosis assay**

269 In order to measure macrophage endocytosis (bulk-phase endocytic ability), FITC-dextran uptake  
270 assay was performed. Following AOH exposure the cells were collected and 5 x 10<sup>5</sup> cells were  
271 incubated at 37 °C for 30 min with FITC-Dextran, 42 kDa (1 mg/ml) and then washed three times  
272 with cold PBS. Cellular uptake of FITC-dextran was measured by flow cytometry (Accuri C6)  
273 using 488<sub>ex</sub>:530/30<sub>em</sub>. A negative control was performed in parallel by incubating cells with

274 FITC-dextran at 4°C instead of 37°C. Uptake of FITC-dextran was expressed as  $\Delta$  median  
275 fluorescence intensity (MFI), i.e., MFI (uptake at 37°C) – MFI (uptake at 4°C). Background  
276 (negative control) was withdrawn and AOH-induced phagocytic activity calculated.

277

## 278 **2.6. RT-PCR**

279 Gene expression of TNF $\alpha$ , IL-6 and IL-12 in RAW 264.7 cells were quantified by RT-PCR using  
280 gene specific primer-probe technology (Life Technologies) as previously described in Solhaug *et*  
281 *al.*, 2012. The following TaqMan<sup>®</sup> probes were used: Mm00443258\_m1 for TNF $\alpha$ ,  
282 Mm00446190\_m1 for IL-6, Mm01288989\_m1 for IL-12p40 and Mm00437762\_m1 for B2M.

283 Gene expression of iNOS and Arg-1 in RAW 264.7 cells were monitored using The TaqMan<sup>®</sup>  
284 Gene Expression Master Mix (Applied Biosystems, Carlsbad, CA) according to the  
285 manufacturer's recommendations and analyzed using a Rotor Gene 6000 Real-Time PCR  
286 Machine (Qiagen, Germantown, MD) as previously described (Christoffersen *et al.*, 2015). The  
287 following TaqMan<sup>®</sup> probes were used: Mm00440502\_m1 for Nos2, Mm00475988\_m1 for Arg1  
288 and Mm02528467\_g1 for Rpl32.

289

## 290 **2.7. Cytokine measurement:**

291 *ELISA*: Following exposure of RAW 264.7 cells, conditioned media was centrifuged (500 g for  
292 10 min) and supernatants collected to remove cell debris. TNF $\alpha$  and IL-6 were quantified by  
293 enzyme-linked immunosorbent (ELISA), according to the manufacturer's guidelines (BD  
294 Biosciences) using a Viktor2 multilabel counter (Perkin Elmer, Boston, MA, USA) equipped  
295 with appropriate software (Magellan VI). Cytokine levels were normalized in regards to cell  
296 number as AOH is found to inhibit RAW 264.7 cell proliferation (Solhaug *et al.*, 2012).

297 *Cytokine bead assay (CBA)*: Following exposure of primary macrophages, conditioned media  
298 were centrifuged at 500 g for 10 min and supernatant collected to remove cell debris. Levels of  
299 IL-12p70, TNF $\alpha$ , IL-10, IL-6, IL-8 and IL-1 $\beta$  were measured simultaneously using CBA and  
300 flow cytometry (Accuri C6), according to the manufacturer's guidelines

301

## 302 **2.8. Cytotoxicity**

303 *Microscopy*: Changes in nuclear morphology and plasma membrane damages were evaluated  
304 after staining cells ( $\sim 0.5 \times 10^6$  cells) with propidium iodide (PI, 10  $\mu$ g/ml) and Hoechst 33342 (5

305  $\mu\text{g/ml}$ ) for 30 min. Stained cells suspended in 10  $\mu\text{l}$  FBS were applied to slides and air-dried.  
306 Nuclear morphology associated with necrosis and apoptosis was determined using a Nikon  
307 Eclipse E400 fluorescence microscope. A minimum of 300 cells were counted per slide.

308 *Flow cytometry:* Necrotic and late apoptotic cells have impaired membrane integrity and cannot  
309 exclude PI like viable cells. Cells were harvested and stained with PI (5  $\mu\text{g/ml}$ ) for 10 min in the  
310 dark at ambient temperature and analyzed immediately by flow cytometry (Accuri C6) using  
311 488<sub>ex</sub>:585/42<sub>em</sub>.

312 *Alamar Blue:* Viability of the primary mouse peritoneal macrophages was measured by Alamar  
313 blue as described in Solhaug *et al.*, 2012.

314

### 315 **2.9. ROS measurements**

316 ROS production was detected using oxidation-sensitive fluorescent probes. H<sub>2</sub>DCFDA-CM (1  
317  $\mu\text{M}$ ) was used to detect H<sub>2</sub>O<sub>2</sub> and DHE (5  $\mu\text{M}$ ) to detect O<sub>2</sub><sup>-</sup>. The cells were harvested and  
318 loaded with H<sub>2</sub>DCFDA-CM or DHE for 20 min at 37 °C under 5% CO<sub>2</sub>. The cells were washed  
319 twice with ice cold PBS and analyzed by flow cytometry (Accuri C6). H<sub>2</sub>DCFDA-CM was  
320 measured by using 488<sub>ex</sub>:530/30<sub>em</sub> and DHE using 488<sub>ex</sub>:585/42<sub>em</sub>. Relative expression was  
321 expressed as MFI. The pro-oxidant H<sub>2</sub>O<sub>2</sub> (1 mM, 10 min) was used as a positive control.

322

### 323 **2.10. Measurement of $\gamma\text{H2AX}$ and LC3II by flow cytometry**

324 Following treatments, cells were harvested, washed once in PBS, fixed in 2% paraformaldehyde  
325 (PFA) in PBS for 10 min on ice, and post-fixed/permeabilized in 90% ice-cold methanol for 24 h  
326 or more at -20 °C. For staining with antibody, 5 x 10<sup>5</sup> cells were washed twice with 0.5% BSA in  
327 PBS and then incubated with  $\gamma\text{H2AX}$  or LC3B antibody in 0.5% BSA/PBS overnight at 4 °C.  
328 Cells were then rinsed twice in 0.5% BSA/PBS and incubated with secondary antibody  
329 conjugated to Alexa Fluor 647 for 2 h at room temperature in the dark. Finally cells were rinsed  
330 twice and analyzed by flow cytometry (Accuri C6) using 633<sub>ex</sub>:675/25<sub>em</sub>. For analysis of cell  
331 cycle distribution in addition to protein expression, the cells were washed with PBS, incubated  
332 with propidium iodide (PI; 10  $\mu\text{g/ml}$ ) / RNase A (100  $\mu\text{g/ml}$ ) in PBS for 30 min at 37 °C before  
333 analyses on a flow cytometer (Accuri C6). Single cells were gated and a minimum of 10,000 cells  
334 acquired and analyzed using 488<sub>ex</sub>:585/40<sub>em</sub> vs 647<sub>ex</sub>:675/25<sub>em</sub>.

335

336 **2.11. Statistical analysis**

337 Data analyses were performed using Sigma Plot version 13.0. Statistical significance ( $p < 0.05$ )  
338 was assessed using 1-way ANOVA, followed by Dunnett's post-test or paired t-test as indicated.

339

340 **3. Results**

341

342 **3.1. AOH induces morphological and phenotypic changes in RAW 264.7 macrophages.**

343 In order to evaluate the effect of AOH on macrophage morphology, RAW 264.7 cells were  
344 treated with AOH (15 and 30  $\mu\text{M}$ ) for 24 h followed by staining of the cytoskeleton and nuclei.  
345 Exposure to 15  $\mu\text{M}$  AOH did not induce any obvious morphological changes (data not shown),  
346 but after exposure to AOH (30  $\mu\text{M}$ ) the morphology changed from small and round into more  
347 flattened cells, others were star-shaped or with elongated spindle shapes (Fig. 1). The  
348 morphological changes were found to be sustained also after 48 h exposure (data not shown). In  
349 agreement with our previous reports (Solhaug *et al.*, 2013), AOH were also found to induce  
350 abnormal nuclei, such as micronuclei and polyploidy (Fig. 1). Little or no cell death was  
351 observed after AOH exposure (Supplementary, Fig. S2), which is in agreement with that AOH  
352 reduce the proliferation rate by the induction of cell cycle arrest rather than cell death (Solhaug *et*  
353 *al.*, 2012, 2013). We have previously shown that AOH increases the cellular level of ROS in  
354 RAW 264.7 cells, and that this ROS was without effects on the AOH-induced cell cycle arrest  
355 (Solhaug *et al.*, 2012). Here, we added the antioxidant N-acetyl-L-cysteine (NAC, 5mM) to  
356 examine if ROS production was linked to the morphological changes. Even though antioxidants  
357 reduce AOH induced ROS production (Solhaug *et al.*, 2012), the addition had no obvious effect  
358 on the AOH-induced changes in cell morphology (Supplementary, Fig S3).

359

360 Next we examined if the observed morphological changes corresponded to potential changes in  
361 cell surface markers expression relevant to macrophage differentiation. In contrast to the  
362 morphological changes, preliminary results showed that phenotypic markers, such as expression  
363 of surface receptors were more clearly up-regulated after 48 h compare to 24 h treatment with  
364 AOH (30  $\mu\text{M}$ ; data not shown). Further studies in order to characterize the phenotypic changes  
365 were therefore performed mainly with 48 h of AOH (30  $\mu\text{M}$ ). As can be seen from the data  
366 presented in Fig. 2, CD86, CD80 and MHCII, important co-stimulatory molecules for T cell

367 activation, were all up-regulated in RAW 264.7 cells after exposure to AOH (30  $\mu$ M). Similarly,  
368 also the expression of the integrin CD11b was found to be up-regulated by AOH. In contrast,  
369 CD83 which is associated with DC maturation was not affected. To investigate if AOH induced  
370 changes of pro-inflammatory cytokines, we measured the expression of TNF $\alpha$ , IL-6 and IL-  
371 12p40 by RT-PCR. Both TNF $\alpha$  and IL-6 mRNA expression were found to be up-regulated in  
372 RAW 264.7 cells (Fig. 3A). IL-12 is composed of two heterologous chains; p40 and p35, which  
373 together form IL-12p70 and is a key cytokine released from immature and mature DCs (Steinman  
374 *et al.*, 2007; Shortman *et al.*, 2007). AOH was not found to induce expression of IL-12p40 in  
375 RAW 264.7 cells (Fig 3A). At the protein level, ELISA confirmed an AOH-induced up-  
376 regulation of TNF $\alpha$  release (Fig. 3B). In contrast, IL-6 could not be detected (data not shown),  
377 which might be caused by effects linked to post-transcriptional changes/ processes induced by  
378 AOH. To further characterize the AOH induced differentiation of the RAW 264.7 cells, we  
379 employed qPCR to measure expression of iNOS and Arg-1 as their up-regulation is commonly  
380 used as indicators for M1 or M2 macrophage polarization in mice, respectively (Stout *et al.*,  
381 2005; Kigerl *et al.*, 2009). However, AOH (30  $\mu$ M, 12-72 h) did not increase the expression of  
382 either iNOS or Arg-1 (data not shown). Endocytosis is required for the intracellular processing  
383 and presentation of exogenous antigenic fragments, and is a crucial function of macrophages as  
384 well as immature DCs. Endocytic capacity of the AOH treated cells was investigated by the  
385 uptake of FITC-dextran. A significantly higher amount of FITC-dextran was taken up by  
386 macrophages treated with AOH (30  $\mu$ M) for 48 h (Fig. 4) compared to untreated cells, indicating  
387 a higher endocytic activity. This was not the case when cells were stimulated with lower  
388 concentrations of AOH (15  $\mu$ M), which corresponds well with the morphological changes  
389 described above.

390

### 391 ***3.2. AOH induces morphological and phenotypically changes in human primary macrophages***

392 To further study the effects of AOH on macrophage morphology, we next investigated if AOH  
393 induced similar morphological changes in primary human macrophages. Human blood  
394 monocytes were differentiated into macrophages by GM-CSF for 7 days, followed by exposure to  
395 AOH (30  $\mu$ M) for 24 h. A dramatic change in morphology was observed in AOH-treated cells  
396 compared to the untreated control after 24 h (Fig. 5A) and 48 h exposure (Fig. 5B). Most cells  
397 appeared elongated with dendrite-like protrusions after AOH-exposure, while untreated cells

398 remained round. The morphological changes were similar after 24 and 48 h AOH (30  $\mu$ M)  
399 exposure. No cell death was observed (Supplementary, Fig. S4). To further characterize the  
400 prominent changes in morphology induced by AOH (30  $\mu$ M, 24 h), we measured the expression  
401 of several surface receptors, commonly associated with M1 (CD80, CD86), M2 (CD200r,  
402 CD163) or DCs (CD83, CD86, HLA-DR) in addition to the more common macrophage marker  
403 CD68. Interestingly, both CD83 and CD86 were found to be up-regulated in response to AOH  
404 treatment while HLA-DR and CD68 were down-regulated (Fig. 6). No significant changes were  
405 detected for CD80, CD200r and CD163 (Fig. 6). To assess the effects of AOH on pro-  
406 inflammatory cytokine production in primary macrophages, the secretion of TNF $\alpha$ , IL-6, IL-8,  
407 IL-1 $\beta$ , IL-10 and IL-12p70 was measured using cytokine bead assay (CBA). AOH induced  
408 increased secretion of TNF $\alpha$  and IL-6, but had no effects on IL-8, IL-1 $\beta$ , IL-10 or IL-12p70  
409 levels (Fig. 7). In RAW 264.7 macrophages AOH were found to increase the endocytic capacity  
410 (Fig. 4). In contrast, the primary macrophages had lower uptake of FITC-dextran when treated  
411 with AOH compared to control (Fig. 8). Interestingly, similar effects of AOH on morphology and  
412 uptake of FITC-dextran, with no effects on cell viability, were observed in AOH-treated primary  
413 peritoneal macrophages isolated from mouse (Supplementary, Fig. S5).

414  
415 Recently, we found that AOH induced autophagy in RAW 264.7 cells (Solhaug *et al.*, 2014).  
416 Thus, as autophagy has been found to be essential during macrophage differentiation (Jacquel *et*  
417 *al.*, 2012), we next examined the level of the autophagosome marker LC3II. In the primary  
418 macrophages exposure to AOH (30  $\mu$ M, 24 h; Fig. 9) resulted in a down-regulation of LC3II,  
419 suggesting reduced autophagy.

420  
421 **3.3 AOH induced ROS, DNA damage and cell cycle arrest in human primary macrophages**  
422 AOH-induced ROS was found to be associated with SSBs and oxidative DNA damage (Solhaug  
423 *et al.*, 2012). Thus, in order to further elucidate possible mechanisms involved in AOH-induced  
424 morphological changes, we next analyzed intracellular ROS levels using H<sub>2</sub>DCFDA-CM and  
425 DHE probes detecting H<sub>2</sub>O<sub>2</sub> and O<sub>2</sub><sup>-</sup>, respectively. In contrast to the RAW 264.7 macrophages  
426 (Solhaug *et al.*, 2012), AOH (30 - 60  $\mu$ M) showed only a slight up-regulation (not significant) of  
427 H<sub>2</sub>O<sub>2</sub> production after 2 h, 6 h and 24 h exposure (Fig. 10AB). No O<sub>2</sub><sup>-</sup> production was detected  
428 after 24 h of AOH exposure (30 - 60  $\mu$ M, data not shown). Furthermore, in accordance with

429 observations in RAW 264.7 cells, addition of the ROS scavenger NAC (5 mM; 24 h) did not  
430 change the AOH-induced morphological changes as evaluated by light microscopy  
431 (Supplementary, Fig. S6).

432  
433 AOH's effects on topoisomerase (Fehr *et al.*, 2009) have been suggested to be linked to an  
434 increased level of DSBs (Solhaug *et al.*, 2012). As increased phosphorylation of H2AX ( $\gamma$ H2AX)  
435 is indicative of DSBs, we next examined  $\gamma$ H2AX expression vs. cell cycle by flow cytometry  
436 (Sordet *et al.*, 2009). As expected, the primary macrophages had only a limited proliferation rate  
437 as only approximately 2% of the cells were found to be in S phase (Fig. 11AD). Despite the low  
438 level of proliferation in these cells, AOH exposure markedly enhanced cell numbers in G<sub>2</sub> (Fig.  
439 11ACD). Most importantly, increased levels of  $\gamma$ H2AX were seen following exposure to AOH  
440 (Fig. 11AB), suggesting an enhanced level of DSBs possibly via its known effect on  
441 topoisomerase. Interestingly,  $\gamma$ H2AX was enhanced in all phases of the cell cycle, suggesting that  
442 inhibition of topoisomerase during replication as well as transcription could cause DSBs (Fig.  
443 11A).

444

#### 445 **4. Discussion**

446 Our previous studies show that AOH induces ROS and DNA damage followed by G<sub>2</sub> arrest in  
447 RAW 264.7 macrophages (Solhaug *et al.*, 2012, 2013). We have also identified AOH as an  
448 inducer of autophagy as well as senescence in these cells (Solhaug *et al.*, 2014). These cellular  
449 effects were suggested to be linked to an AOH-initiating effect on topoisomerase thereby causing  
450 DSBs, rather than enhanced ROS (Solhaug *et al.*, 2012, 2014). In the present study, we find that  
451 AOH modified the phenotype of proliferating RAW 264.7 and the slowly proliferating primary  
452 human macrophages. The AOH-induced changes on morphology and inflammatory cytokine  
453 responses were rather similar in the two models. In contrast, the effects of AOH with regard to  
454 endocytosis, autophagy as well as expression of CD-markers were markedly different (Table 1).  
455 The phenotypes did neither match with typical M1/ M2 macrophages nor with DC.

456

457 Plasticity and functional polarization are hallmarks of macrophages. Here we find that AOH  
458 induced star-shaped morphology of the RAW 264.7 cells. Similar morphological changes have  
459 been previously reported and associated with macrophage differentiation into DCs (Saxena *et al.*,

460 2003; Lee *et al.*, 2004). In this study, the levels of CD80, CD86, MHCII and CD11b were  
461 increased, as here also seen in AOH-exposed cells. In contrast, the expression of CD83, a marker  
462 of DC differentiation and maturation, was found to be unchanged after AOH exposure.  
463 Furthermore, AOH did not induce expression of IL-12p40, which is a key cytokine released from  
464 immature and mature DCs (Steinman *et al.*, 2007; Shortman *et al.*, 2007). Although, the changes  
465 in cell surface marker expression and enhanced endocytic activity shows that AOH exposure  
466 induced marked phenotypical changes in the macrophages. The AOH treated RAW 264.7  
467 macrophages displayed several of the M1 characteristics, such as increased expression of MHCII,  
468 CD80, CD86 and increased secretion of TNF $\alpha$ . On the other hand, AOH did not enhance the  
469 expression of iNOS or release of IL-12p70, and the differentiated macrophages can therefore not  
470 be characterized as classical M1 macrophages. Similarly, the typical characteristics of M2  
471 macrophages, such as elongated morphology (Bolling *et al.*, 2012) and expression of IL-10 and  
472 Arg-1, were not fulfilled. Thus, the RAW 264.7 cells obtained after AOH exposure cannot be  
473 categorized as classical DC or as M1/ M2 macrophages.

474  
475 In the primary human macrophage model, AOH induced even more DC-like morphology with  
476 elongated cells showing dendrite-like protrusions. Similar to what was seen in the RAW 264.7  
477 cells, AOH also modifies the phenotype of the primary macrophages. More specifically, the  
478 AOH-exposed primary human macrophages show increased expression of CD83 and CD86  
479 together with decreased CD68 levels, increased secretion of TNF $\alpha$  and IL-6 and decreased  
480 endocytosis, which may represent modifications into a more DC-like phenotype. On the other  
481 hand, rather a down regulation of HLA-DR and no increased secretion of IL-12p70 were found.  
482 As seen with the RAW 264.7 model, the phenotypically characteristic of the AOH treated  
483 primary macrophages did not fit with DC, M1 nor M2 polarized macrophages.

484  
485 It is important to note that the DC and M1/M2 classification scheme of macrophages is generally  
486 considered to be an oversimplification of the true spectrum of macrophage phenotypes (Wermuth  
487 and Jimenez, 2015). Thus, it is not surprising that the changes seen following exposure to a  
488 cellular stressor like the mycotoxin AOH could not be clearly categorized. The interesting and  
489 important part is that AOH did change the morphology and the macrophage phenotype in the  
490 experimental models tested, RAW 264.7 mouse macrophages, primary human macrophages and

491 primary mouse peritoneal macrophages (Supplementary, Fig. S5). Although the macrophages  
492 exposed were in different stage of differentiation due to their diverse origin. The macrophages  
493 response to AOH could have potentially important implications as the proper function of tissue  
494 macrophages and DCs are essential for the health of specialized parenchymal and stromal cells  
495 (Mills and Ley, 2014). Possible theoretical implications could be a decrease of immune response  
496 in case of infections and/or a disturbed balance of the adaptive immune system.

497  
498 There have been reports linking exposure to various mycotoxins to changes in macrophage  
499 phenotype and/or effects on the differentiation processes of monocytes to macrophages (Wache  
500 *et al.*, 2009; Gammelsrud *et al.*, 2012; Ficheux *et al.*, 2013). More specific, deoxynivalenol, a  
501 *Fusarium* mycotoxin, inhibits INF- $\gamma$  mediated macrophage activation, assessed by the expression  
502 of several surface receptors, when the cells are exposed during the differentiation process from  
503 monocytes to macrophages (Wache *et al.*, 2009). Furthermore, monocytes exposed to enniatin B,  
504 another *Fusarium* mycotoxin, during the differentiation process into macrophages presented a  
505 decrease of endocytosis and an increase of CD71 (Ficheux *et al.*, 2013). Interestingly, enniatin B  
506 exposed to RAW 264.7 macrophages were also found to induce expression of CD163, a marker  
507 for M2 macrophages (Gammelsrud *et al.*, 2012). To our knowledge, this is the first study  
508 describing morphological and phenotypical changes induced by AOH on macrophages.

509  
510 Various cellular processes have been associated to the macrophage differentiation development,  
511 from specific interactions with specific cellular receptors (Martinez and Gordon, 2014) to more  
512 unspecific processes including DNA damage responses (So *et al.*, 2013) and autophagy (Jacquel  
513 *et al.*, 2012). Less is known with regard to important initial molecular events triggering these  
514 changes. There are reports suggesting a crucial role for ROS (Nakanishi *et al.*, 2013) and NO  
515 (Nogueira-Pedro *et al.*, 2014). We recently reported that AOH could be a potent inducer of ROS  
516 in the RAW 264.7 macrophage model (Solhaug *et al.*, 2012). However, here in this study,  
517 we found that a potent anti-oxidant (NAC) did not reduce the AOH-induced morphological  
518 changes. Furthermore, AOH induced differentiation of primary humane macrophages in the  
519 apparent absence of ROS formation. Hence, ROS does not seem to be an obligatory part of  
520 macrophage differentiation induced by AOH.

521

522 The other primary initiating molecular event of AOH presently known is an interaction with  
523 topoisomerase (Fehr *et al.*, 2009). In general, interactions with topoisomerase often result in  
524 DSBs as a consequence of the delayed replicative and/or transcriptional syntheses (Durand-  
525 Dubief *et al.*, 2014, Sordet *et al.*, 2009). In our recent study, we observed that AOH exposure  
526 resulted in increased  $\gamma$ H2AX, and suggested that AOH-induced DSBs were an important  
527 triggering signal for G<sub>2</sub> arrest and autophagy (Solhaug *et al.*, 2012, 2014). Also in the primary  
528 human macrophage model, AOH is suggested to increase  $\gamma$ H2AX as a DNA damage response  
529 caused by DSBs.  $\gamma$ H2AX was enhanced in all phases of the cell cycle, suggesting that inhibition  
530 of topoisomerase during replication as well as transcription could cause DSBs. Most  
531 interestingly, differentiation has been suggested as an outcome in response to DSBs (Sherman *et*  
532 *al.*, 2011). Furthermore, DNA damaging agents is found to alter the differentiation-process of  
533 monocytes to favour the generation of M2 macrophages (Dijkgraaf *et al.*, 2013). DNA damage  
534 has also been suggested to be an important mediator in the decision of hematopoietic stem cells  
535 to exit quiescence and to differentiate (Weiss and Ito, 2015). Differentiation is typical tightly  
536 linked to cell cycle withdrawal (Rots *et al.*, 1999). Thus, we first hypothesized that increased  
537 DSBs could result in a G<sub>2</sub> arrest, linked to a changed phenotype. However, in contrast to AOH-  
538 exposed RAW 264.7 cells, the primary human macrophages were found to be only slowly  
539 proliferating and the majority of the cells were in G<sub>1</sub> phase. Thus, there are obviously no direct  
540 link between the AOH-induced macrophage differentiation and a specific cell cycle arrest.  
541 However, a link between AOH induced DNA damage and changes in macrophage morphology  
542 and phenotype is still plausible.

543  
544 Autophagy (macro-autophagy) is a re-cycling mechanism by which cells through lysosomal  
545 degradation reuse amino- and fatty acids. Interestingly, autophagy has been reported to be  
546 essential during the differentiation process from monocytes to macrophages, which require  
547 marked architectural remodelling (Jacquel *et al.*, 2012; Zhang *et al.*, 2012). Furthermore,  
548 autophagy has been found to be important in differentiation and polarization of macrophages.  
549 However, the precise role of autophagy is still uncertain and it has been suggested to be a both a  
550 positive and negative regulator of M1 differentiation (Jung *et al.*, 2010; Chen *et al.*, 2014; Liu *et*  
551 *al.*, 2015). Here we find that AOH-induced morphological changes in the RAW 264.7 cells,  
552 previously shown to have increased DSBs and increased autophagy; whereas AOH reduced

553 autophagy in the primary human macrophages. This supports the notion that there is no clear  
554 relationship between autophagy and macrophage differentiation/ polarization process. There  
555 seems to be rather complex signalling interactions on-going between autophagy and the  
556 macrophage differentiation process, as inhibition of AOH-induced autophagy caused increased  
557 cell death rather than influence the degree of morphological changes in RAW 264.7 cells  
558 (Solhaug *et al.*, 2014).

559  
560 The concentrations of AOH used in this study are in the same range that causing DNA damage as  
561 previously published by us (Solhaug *et al.*, 2012) and others (Brugger *et al.*, 2006; Fehr *et al.*,  
562 2009; Pfeiffer *et al.*, 2007). Current knowledge concerning adverse effects of AOH in humans  
563 and animals are still limited. An *in vivo* mouse study done by Schuchardt and co-workers (2014)  
564 showed that uptake of AOH over the gut were somewhat poor. However, this can be different for  
565 other species and/or with other prolonged feeding trails. An ongoing inflammation in the gut may  
566 also increase the uptake as well as the effect. Thus an uptake of AOH at levels that may affect the  
567 immune system cannot be excluded.

568  
569 **Conclusion**  
570 The present study show that AOH induced marked phenotypic changes in macrophages. These  
571 changes could not be directly linked to an initial AOH-induced ROS production, cell cycle arrest  
572 or autophagy as seen as a consequence of AOH-induced DSBs. However, AOH-induced DSBs  
573 will result in a complex DNA damage response and a link towards macrophage differentiation is  
574 still a likely explanation.

575  
576  
577 **Conflicts of interest statement**

578 The authors declare that there are no conflicts of interest.  
579

580 **Acknowledgements**  
581 The authors wish to thank Dr. Charlotte Kleiveland (Department of Chemistry, Biotechnology  
582 and Food Science, Norwegian University of Life Sciences, Aas, Norway) and Laura L. Vines  
583 (Michigan State University, Department of Food Science and Human Nutrition, East Lansing,

584 MI, USA) for practical assistance in the laboratory. The work has been supported by The  
585 Research Council of Norway through the project Toxicological characterization of selected  
586 secondary fungal metabolites in grain, grant nr.: 185622/V40. We also wish to thank the research  
587 group, FUNtox, at the Norwegian Veterinary Institute, for additional funding.

588

589 **Figure legends:**

590

591 **Figure 1: AOH induces morphological changes in RAW 264.7 cells.** Cells were exposed to  
592 AOH (30  $\mu$ M) or left untreated for 24 h before staining the actin filaments and DNA with  
593 Phalloidin Alexa Fluor 555 (upper) or Hoechst (lower), respectively, followed by fluorescent  
594 microscopy. \* Micronuclei. \*\* Polyploidy.

595

596 **Figure 2: Expression of cell surface receptors following AOH-exposure in RAW 264.7 cells.**  
597 RAW 264.7 cells were treated with 30  $\mu$ M AOH for 48 h and analyzed for the expression of  
598 CD86, CD80, CD83, MHCII and CD11b surface molecules by flow cytometry. Mean values  $\pm$   
599 SEM of 4-6 independent experiments are presented. \* indicates significantly different from  
600 control,  $p < 0.05$  (1-way-ANOVA with Dunnett`s post-test).

601

602 **Figure 3: Effects of AOH on TNF $\alpha$ , IL-12 and IL-6 cytokine production in RAW 264.7 cells.**  
603 (A) RAW 264.7 cells were treated with AOH (30  $\mu$ M) or left untreated for 48 h. Gene expression  
604 of TNF $\alpha$ , IL-12p40 and IL-6 were analyzed by qRT-PCR. Two independent experiments using  
605 biological triplicates were performed. The results were statistically assessed using one-way  
606 ANOVA with Dunnett`s post-test. (B) RAW 264.7 cells were treated with AOH (30  $\mu$ M) or left  
607 untreated for 6 - 48 h and analyzed for TNF $\alpha$  secretion by ELISA. The results represent the mean  
608 values  $\pm$  SD of 3 independent incubations.\* indicates significantly different from control,  $p <$   
609 0.05 (1-way-ANOVA with Dunnett`s post-test).

610

611 **Figure 4: Alterations in endocytic activity induced by AOH in RAW 264.7 cells.** RAW 264.7  
612 cells were left untreated or treated with AOH at the concentrations indicated for 48 h and  
613 analyzed for FITC-dextran uptake by flow cytometry (A). The results represent mean values  $\pm$

614 SEM of 3 independent experiments (B). \* indicates significantly different from control,  $p > 0.05$   
615 (1-way-ANOVA with Dunnett`s post-test).

616  
617 **Figure 5: AOH induces morphological changes in human primary macrophages.** (A) Human  
618 primary macrophages were exposed to AOH (30  $\mu\text{M}$ ) or left untreated for 24 h and the actin  
619 filaments were stained with Phalloidin Alexa Fluor 555 (upper) and the nuclei stained with  
620 Hoechst (lower) prior to fluorescence microscopic analysis. (B) Human primary macrophages  
621 were exposed to AOH (30  $\mu\text{M}$ ) or left untreated for 48 h and analyzed by SEM.

622  
623 **Figure 6: Phenotypic characterization of AOH-treated human primary macrophages.** Cells  
624 were treated with AOH (30  $\mu\text{M}$ ) or left untreated for 24 h and analyzed for the expression of  
625 CD80, CD200r, CD163, CD83, CD86, HLA-DR or CD68 by flow cytometry (A). The relative  
626 expression is quantified as MFI and the results represent mean values  $\pm$  SEM of 3-5 independent  
627 experiments (B). \* indicates significantly different from control,  $p < 0.05$  (1-way-ANOVA with  
628 Dunnett`s post-test).

629  
630 **Figure 7: AOH induces cytokine secretion in human primary macrophages.** Cells were  
631 treated with 30  $\mu\text{M}$  AOH or left untreated for 24 h and the supernatant analyzed for cytokine  
632 secretion (IL-12p70,  $\text{TNF}\alpha$ , IL-10, IL-6, IL-8 and IL-1 $\beta$ ) by CBA. The results represent mean  
633 values  $\pm$  SEM of 3 independent incubations, representative of 9 different experiments. \* indicates  
634 significantly different from control,  $p < 0.05$  (1-way-ANOVA with Dunnett`s post-test).

635  
636 **Figure 8: Endocytic activity induced by AOH in human primary macrophages.** Cells were  
637 treated with 30  $\mu\text{M}$  AOH or left untreated for 24 h and analyzed for FITC-dextran uptake by flow  
638 cytometry (A). The relative expression is quantified as MFI. The results represent mean values  $\pm$   
639 SEM of 4 independent experiments (B). \* indicates significantly different from control,  $p < 0.05$   
640 (1-way-ANOVA with Dunnett`s post-test).

641  
642 **Figure 9: Expression of LC3II in response to AOH in human primary macrophages.** Cells  
643 were treated with 30  $\mu\text{M}$  AOH or left untreated for 24 h and analyzed for LC3II expression by  
644 flow cytometry. The relative expression is quantified as MFI. The results represent mean values  $\pm$

645 SEM of 3 independent experiments. \* indicates significantly different from control,  $p < 0.05$  (1-  
646 way-ANOVA with Dunnett`s post-test).

647  
648 **Figure 10: AOH induced ROS in human primary macrophages.** Cells were treated with AOH  
649 (30 and 60  $\mu\text{M}$ ) or left untreated and analyzed for ROS production after 2, 6 and 24 h by flow  
650 cytometry. Positive ctrl (PC):  $\text{H}_2\text{O}_2$  (1 mM, 10 min). The results are representative for 3  
651 independent experiments (A). The relative expression is quantified as MFI. The results represent  
652 mean values  $\pm$  SEM of 3 independent experiments (B). \* indicates significantly different from  
653 control,  $p < 0.05$  (1-way-ANOVA with Dunnett`s post-test).

654  
655 **Figure 11: AOH induced DNA damage in human primary macrophages.** The cells were  
656 treated with AOH at the indicated concentrations or left untreated for 6 or 24 h and analyzed for  
657  $\gamma\text{H2AX}$  expression and cell cycle by flow cytometry. (A) Events above the dotted line represent  
658 cells positive for  $\gamma\text{H2AX}$ , while the x-axis represent DNA content (cell cycle distribution). (B)  
659 Quantification of  $\gamma\text{H2AX}$  positive cells. (C) Cell cycle distribution in response to AOH 30  $\mu\text{M}$ ,  
660 24 h exposure. (D) Quantification of cell cycle distribution. The results represent mean values  $\pm$   
661 SEM of 3 independent experiments. \* indicates significantly different from control,  $p < 0.05$  (B:  
662 1-way-ANOVA with Dunnett`s post-test, D: paired t-test).

663  
664 **Supplementary:**

665  
666 **Figure S1: Human monocyte-macrophage differentiation.** (A) GM-CSF induced  
667 differentiation of primary human monocytes into macrophages. Pictures are taken after 1 or 7  
668 days. (B) Flow cytometric characterization of monocyte/macrophage purity and differentiation  
669 after 1 (upper) and 7 days of GM-CSF treatment. Black line: Isotype control, Red line: CD68

670  
671 **Figure S2: AOH induced cell death in RAW 264.7 cells.** RAW 264.7 cells were treated with  
672 AOH (60  $\mu\text{M}$ ) or left untreated for 48 h and analyzed for cell death; necrosis and apoptosis by  
673 PI/Hoechst 33342 staining and fluorescence microscopy. The data represent mean of 2  
674 independent experiments.

675

676 **Figure S3: Effects of NAC on AOH induced morphology in RAW 264.7 cells.** The cells were  
677 treated with AOH (30  $\mu$ M) for 24 h in the presence or absence of NAC (5 mM) or left untreated.  
678 The cell morphology was evaluated by light microscopy. The results are representative for 3  
679 independent experiments.

680  
681 **Figure S4: AOH induced cell death in human primary macrophages.** The cells were treated  
682 with AOH at the indicated concentrations or left untreated for 24 h before PI-staining and flow  
683 cytometry. The data represent one of three representative experiments, mean values  $\pm$  SE of 3  
684 independent incubations.

685  
686 **Figure S5: AOH induces morphological changes in primary mouse peritoneal macrophages.**  
687 The cells were exposed to AOH at the concentrations indicated for 48 h or left untreated,  
688 and analyzed by light microscopy (A), for viability by Alamar Blue (B) and for endocytic activity  
689 (C). The data represent one experiment, representative of 2 independent experiments. The  
690 viability results represent mean  $\pm$  SD of 3 independent incubations.

691 **Figure S6: Effects of antioxidants on AOH induced morphology in human primary**  
692 **macrophages.** The cells were treated with AOH (30  $\mu$ M) for 24 h in the presence or absence of  
693 NAC (5 mM) or left untreated. The cell morphology was evaluated by light microscopy. The  
694 results are representative for 2 independent experiments.

695

696

697 **References:**

698 Ackermann, Y., Curtui, V., Dietrich, R., Gross, M., Latif, H., Martlbauer, E., Usleber, E., 2011.  
699 Widespread occurrence of low levels of alternariol in apple and tomato products, as  
700 determined by comparative immunochemical assessment using monoclonal and  
701 polyclonal antibodies. *J.Agric. Food Chem.* **59**, 6360-6368.  
702 Ambarus, C.A., Krausz, S., van Eijk, M., Hamann, J., Radstake, T.R., Reedquist, K.A., Tak, P.P.,  
703 Baeten, D.L., 2012. Systematic validation of specific phenotypic markers for in vitro  
704 polarized human macrophages. *Journal of immunological methods* **375**, 196-206.  
705 Auffray, C., Sieweke, M.H., Geissmann, F., 2009. Blood monocytes: development,  
706 heterogeneity, and relationship with dendritic cells. *Annual review of immunology* **27**,  
707 669-692.  
708 Bain, C.C., Mowat, A.M., 2014. The monocyte-macrophage axis in the intestine. *Cellular*  
709 *immunology* **291**, 41-48.

- 710 Biswas, S.K., Chittechath, M., Shalova, I.N., Lim, J.Y., 2012. Macrophage polarization and  
711 plasticity in health and disease. *Immunologic research* **53**, 11-24.
- 712 Bolling, A.K., Ovrevik, J., Samuelsen, J.T., Holme, J.A., Rakkestad, K.E., Mathisen, G.H.,  
713 Paulsen, R.E., Korsnes, M.S., Becher, R., 2012. Mono-2-ethylhexylphthalate (MEHP)  
714 induces TNF-alpha release and macrophage differentiation through different signalling  
715 pathways in RAW264.7 cells. *Toxicol. Lett.* **209**, 43-50.
- 716 Chen, P., Cescon, M., Bonaldo, P., 2014. Autophagy-mediated regulation of macrophages and its  
717 applications for cancer. *Autophagy* **10**, 192-200.
- 718 Christoffersen, T.E., Olsen Hult, L.T., Solberg, H., Bakke, A., Kuczkowska, K., Huseby, E.,  
719 Jacobsen, M., Lea, T., Kleiveland, C.R., 2015. Effects of the non-commensal  
720 *Methylococcus capsulatus* Bath on mammalian immune cells. *Molecular immunology* **66**,  
721 107-116.
- 722 Coombes, J.L., Powrie, F., 2008. Dendritic cells in intestinal immune regulation. *Nature reviews.*  
723 *Immunology* **8**, 435-446.
- 724 Dijkgraaf, E.M., Heusinkveld, M., Tummers, B., Vogelpoel, L.T., Goedemans, R., Jha, V.,  
725 Nortier, J.W., Welters, M.J., Kroep, J.R., van der Burg, S.H., 2013. Chemotherapy alters  
726 monocyte differentiation to favor generation of cancer-supporting M2 macrophages in the  
727 tumor microenvironment. *Cancer research* **73**, 2480-2492.
- 728 Durand-Dubief, M., Svensson, J.P., Persson, J., Ekwall, K., 2011. Topoisomerases, chromatin  
729 and transcription termination. *Transcription* **2:2**, 66-70.
- 730 EFSA., 2011. Scientific Opinion on the risks for animal and public health related to the presence  
731 of *Alternaria* toxins in feed and food. *EFSA Journal* **9**, 2407.
- 732 Fehr, M., Pahlke, G., Fritz, J., Christensen, M.O., Boege, F., Altemoller, M., Podlech, J., Marko,  
733 D., 2009. Alternariol acts as a topoisomerase poison, preferentially affecting the  $\alpha$   
734 isoform. *Mol. Nutr. Food. Res.* **53**, 441-451.
- 735 Ficheux, A.S., Sibiril, Y., Parent-Massin, D., 2013. Effects of beauvericin, enniatin b and  
736 moniliformin on human dendritic cells and macrophages: an in vitro study. *Toxicol.* **71**, 1-  
737 10.
- 738 Gammelsrud, A., Solhaug, A., Dendele, B., Sandberg, W.J., Ivanova, L., Kochbach, B.A.,  
739 Lagadic-Gossman, D., Refsnes, M., Becher, R., Eriksen, G., Holme, J.A., 2012. Enniatin  
740 B-induced cell death and inflammatory responses in RAW 264.7 murine macrophages.  
741 *Toxicol. Appl. Pharmacol.* **261**, 74-87.
- 742 Hume, D.A., 2008. Differentiation and heterogeneity in the mononuclear phagocyte system.  
743 *Mucosal immunology* **1**, 432-441.
- 744 Jacquelin, A., Obba, S., Solary, E., Auberger, P., 2012. Proper macrophagic differentiation requires  
745 both autophagy and caspase activation. *Autophagy* **8**, 1141-1143.
- 746 Jenkins, S.J., Ruckerl, D., Cook, P.C., Jones, L.H., Finkelman, F.D., van, R.N., MacDonald, A.S.,  
747 Allen, J.E., 2011. Local macrophage proliferation, rather than recruitment from the blood,  
748 is a signature of TH2 inflammation. *Science* **332**, 1284-1288.
- 749 Jensen, S.S., Gad, M., 2010. Differential induction of inflammatory cytokines by dendritic cells  
750 treated with novel TLR-agonist and cytokine based cocktails: targeting dendritic cell in  
751 autoimmunity. *Journal of Inflammation* **7:37**
- 752 Jung, C.H., Ro, S.H., Cao, J., Otto, N.M., Kim, D.H., 2010. mTOR regulation of autophagy.  
753 *FEBS Lett* **584**, 1287-1295.
- 754 Kigerl, K.A., Gensel, J.C., Ankeny, D.P., Alexander, J.K., Donnelly, D.J., Popovich, P.G., 2009.  
755 Identification of Two Distinct Macrophage Subsets with Divergent Effects Causing either

756 Neurotoxicity or Regeneration in the Injured Mouse Spinal Cord. The Journal of  
757 Neuroscience **29**, 13435-13444.

758 Koning, N., van Eijk, M., Pouwels, W., Brouwer, M.S., Voehringer, D., Huitinga, I., Hoek, R.M.,  
759 Raes, G., Hamann, J., 2010. Expression of the inhibitory CD200 receptor is associated  
760 with alternative macrophage activation. Journal of innate immunity **2**, 195-200.

761 Laskin, D.L., Sunil, V.R., Gardner, C.R., Laskin, J.D., 2011. Macrophages and tissue injury:  
762 agents of defense or destruction? Annual review of pharmacology and toxicology. **51**,  
763 267-288.

764 Lee, Y.N., Lee, H.Y., Kang, H.K., Kwak, J.Y., Bae, Y.S., 2004. Phosphatidic acid positively  
765 regulates LPS-induced differentiation of RAW264.7 murine macrophage cell line into  
766 dendritic-like cells. Biochem.Biophys.Res.Commun. **318**, 839-845.

767 Liu, K., Zhao, E., Ilyas, G., Lalazar, G., Lin, Y., Haseeb, M., Tanaka, K.E., Czaja, M.J., 2015.  
768 Impaired macrophage autophagy increases the immune response in obese mice by  
769 promoting proinflammatory macrophage polarization. Autophagy **11**, 271-284.

770 Mantovani, A., Sica, A., Sozzani, S., Allavena, P., Vecchi, A., Locati, M., 2004. The chemokine  
771 system in diverse forms of macrophage activation and polarization. Trends in  
772 immunology **25**, 677-686.

773 Maresca, M., Fantini, J., 2010. Some food-associated mycotoxins as potential risk factors in  
774 humans predisposed to chronic intestinal inflammatory diseases. Toxicon **56**, 282-294.

775 Martinez, F.O., Gordon, S., 2014. The M1 and M2 paradigm of macrophage activation: time for  
776 reassessment. F1000prime reports **6**, 13.

777 Mills, C.D., Ley, K., 2014. M1 and M2 macrophages: the chicken and the egg of immunity.  
778 Journal of innate immunity. **6**, 716-726.

779 Mowat. A.M., Bain, C.C., 2011. Mucosal macrophages in intestinal homeostasis and  
780 inflammation. Journal innate immunity. **3**(6):550-54.

781 Nakanishi, A., Hie, M., Iitsuka, N., Tsukamoto, I., 2013. A crucial role for reactive oxygen  
782 species in macrophage colony-stimulating factor-induced RANK expression in  
783 osteoclastic differentiation. International journal of molecular medicine **31**, 874-880.

784 Nogueira-Pedro, A., Dias, C.C., Regina, H., Segreto, C., Addios, P.C., Lungato, L., D'Almeida,  
785 V., Barros, C.C., Higa, E.M., Buri, M.V., Ferreira, A.T., Paredes-Gamero, E.J., 2014.  
786 Nitric oxide-induced murine hematopoietic stem cell fate involves multiple signaling  
787 proteins, gene expression, and redox modulation. Stem cells **32**, 2949-2960.

788 Ostry, V., 2008. Alternaria mycotoxins: an overview of chemical characterization, producers,  
789 toxicity, analysis and occurrence in foodstuffs. World Mycotoxin Journal **1**, 175-188.

790 Pestka, J.J., 2010. Deoxynivalenol: mechanisms of action, human exposure, and toxicological  
791 relevance. Arch Toxicol. **84**, 663-679.

792 Pfeiffer, E., Eschbach, S., Metzler, M., 2007. Alternaria toxins: DNA strand-breaking activity in  
793 mammalian cells in vitro. Mycotoxin Research. **23**, 152-157.

794 Rots, N.Y., Iavarone, A., Bromleigh, V., Freedman, L.P., 1999. Induced differentiation of U937  
795 cells by 1,25-dihydroxyvitamin D3 involves cell cycle arrest in G1 that is preceded by an  
796 transient proliferative burst and an increase in cyclin expression. Blood. **93**, 2721-2729.

797 Saxena, R.K., Vallyathan, V., Lewis, D.M., 2003. Evidence for lipopolysaccharide-induced  
798 differentiation of RAW264.7 murine macrophage cell line into dendritic like cells.  
799 J.Biosci. **28**, 129-134.

800 Schuchardt, S., Ziemann, C., Hansen, T., 2014. Combined toxicokinetic and *in vivo* genotoxicity  
801 study on *Alternaria* toxins. EFSA supporting publication 2014:EN-679, 130 pp.

802 Sherman, M.H., Bassing, C.H., Teitell, M.A., 2011. Regulation of cell differentiation by the  
803 DNA damage response. *Trends in cell biology* **21**, 312-319.

804 Shortman, K., Naik, S.H., 2007. Steady-state and inflammatory dendritic-cell development. *Nat.*  
805 *Rev. Immunol.* **7(1)**: 19-30.

806 So, E.Y., Kozicki, M., Ouchi, T., 2013. Roles of DNA Damage Response Proteins in Mitogen-  
807 Induced Thp-1 Differentiation into Macrophage. *Journal of cancer biology & research* **1**.

808 Solhaug, A., Vines, L.L., Ivanova, L., Spilsberg, B., Holme, J.A., Pestka, J., Collins, A., Eriksen,  
809 G.S., 2012. Mechanisms involved in alternariol-induced cell cycle arrest. *Mutation*  
810 *research* **738-739**, 1-11.

811 Solhaug, A., Holme, J.A., Haglund, K., Dendele, B., Sergent, O., Pestka, J., Lagadic-Gossmann,  
812 D., Eriksen, G.S., 2013. Alternariol induces abnormal nuclear morphology and cell cycle  
813 arrest in murine RAW 264.7 macrophages. *Toxicol. Lett.* **219**, 8-17.

814 Solhaug, A., Torgersen, M.L., Holme, J.A., Lagadic-Gossmann, D., Eriksen, G.S., 2014.  
815 Autophagy and senescence, stress responses induced by the DNA-damaging mycotoxin  
816 alternariol. *Toxicology* **326**, 119-129.

817 Sordet, O., Redon, C.E., Guirouilh-Barbat, J., Smith, S., Solier, S., Douarre, C., Conti, C.,  
818 Nakamura, A.J., Das, B.B., Nicolas, E., Kohn, K.W., Bonner, W.M., Pommier, Y., 2009.  
819 Ataxia telangiectasia mutated activation by transcription- and topoisomerase I-induced  
820 DNA double-strand breaks. *EMBO reports* **10**, 887-893.

821 Steinman, R.M., Banchereau, J., 2007. Taking dendritic cells into medicine. *Nature* **449(27)**:419-  
822 426.

823 Stout, R.D., Jiang, C., Matta, B., Tietzel, I., Watkins, S.K., Suttles, J., 2005. Macrophages  
824 Sequentially Change Their Functional Phenotype in Response to Changes in  
825 Microenvironmental Influences. *The Journal of Immunology* **175**, 342-349.

826 Uhlig, S., Eriksen, G.S., Hofgaard, I.S., Krska, R., Beltran, E., Sulyok, M., 2013. Faces of a  
827 changing climate: semi-quantitative multi-mycotoxin analysis of grain grown in  
828 exceptional climatic conditions in norway. *Toxins* **5**, 1682-1697.

829 Vos, S.M., Tretter, E.M., Schmidt, B.H., Berger, J.M., 2011. All tangled up: how cells direct,  
830 manage and exploit topoisomerase function. *Nat. Rev. Mol. Cell. Biol.* **12**, 827-841.

831 Waché, Y.J., Hbabi-Haddioui, L., Guzylack-Piriou, L., Belkhef, H., Roques, C., Oswald, I.P.,  
832 2009. The mycotoxin deoxynivalenol inhibits the cell surface expression of activation  
833 markers in human macrophages. *Toxicology* **262**, 239-244.

834 Weiss, C.N., Ito, K., 2015. DNA Damage: A Sensible Mediator of the Differentiation Decision in  
835 Hematopoietic Stem Cells and in Leukemia. *International journal of molecular sciences*  
836 **16**, 6183-6201.

837 Wermuth, P.J., Jimenez, S.A., 2015. The significance of macrophage polarization subtypes for  
838 animal models of tissue fibrosis and human fibrotic diseases. *Clinical and translational*  
839 *medicine* **4**, 2.

840 Wu, F., Groopman, J.D., Pestka, J.J., 2014. Public health impacts of foodborne mycotoxins.  
841 *Annual review of food science and technology* **5**, 351-372.

842 Zhang, Y., Morgan, M.J., Chen, K., Choksi, S., Liu, Z.G., 2012. Induction of autophagy is  
843 essential for monocyte-macrophage differentiation. *Blood* **119**, 2895-2905.

844 Zhou, L.J., Tedder, T.F., 1996. CD14+ blood monocytes can differentiate into functionally  
845 mature CD83+ dendritic cells. *Proc. Natl. Acad. Sci. U S A* **19**;93(6):2588-92.

847



Fig. 1, single column

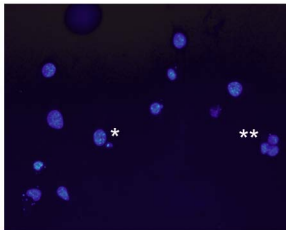
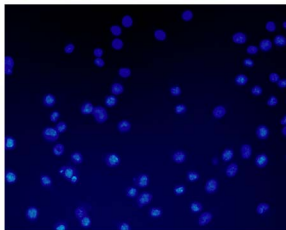
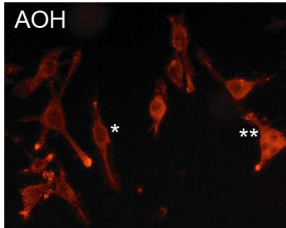
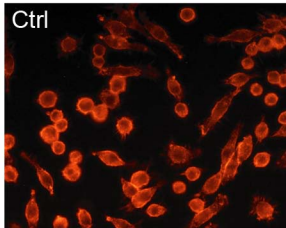


Fig. 2, single column

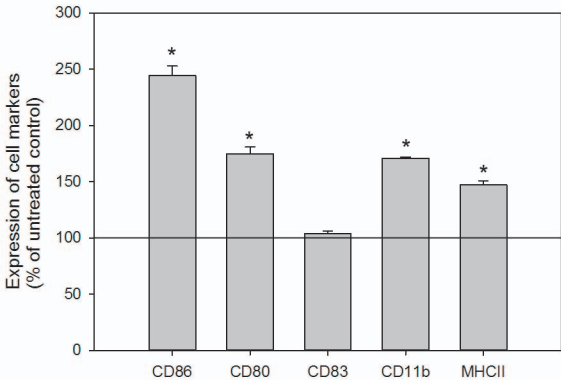
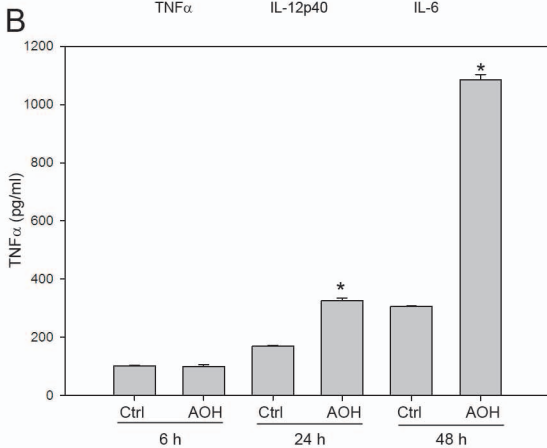
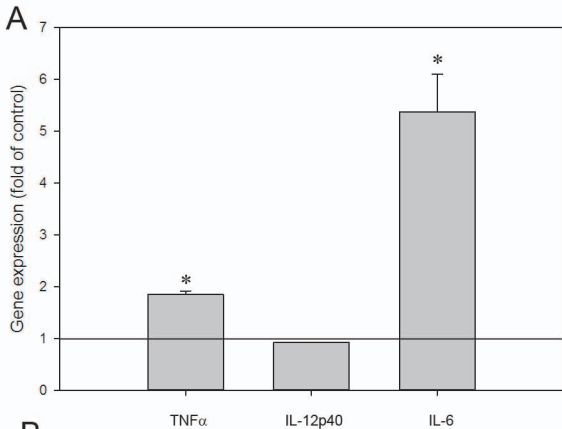


Fig 3, single column



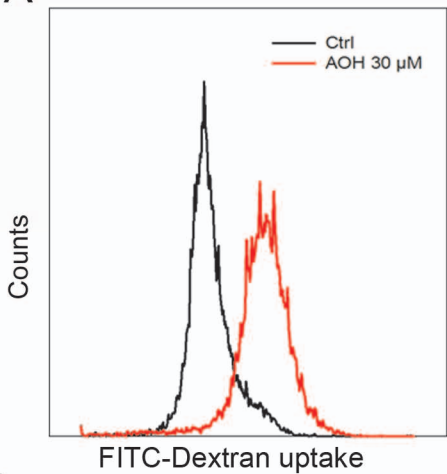
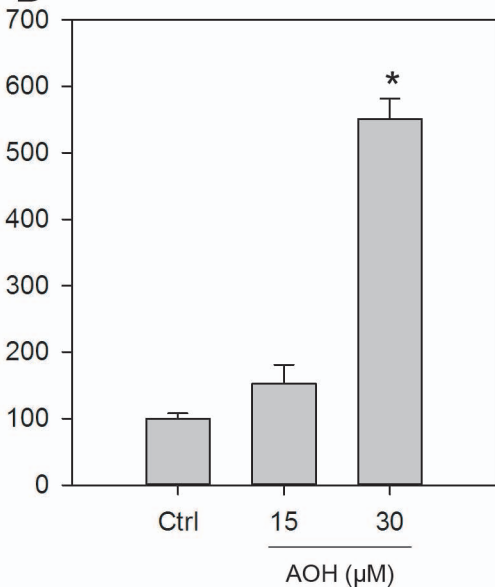
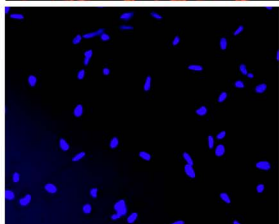
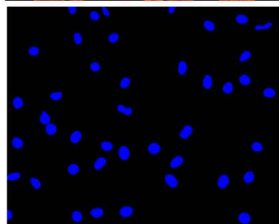
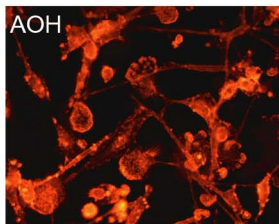
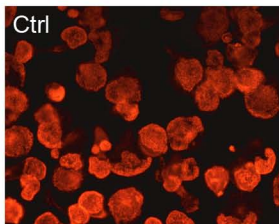
**A****B**

Fig 5, single column

A



B

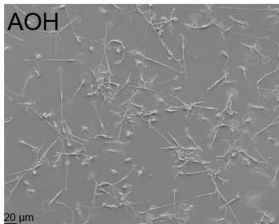
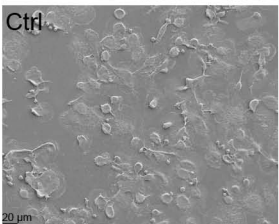
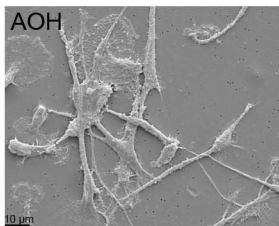
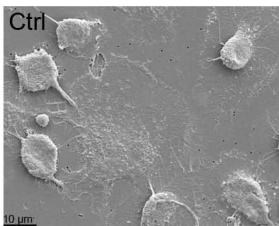
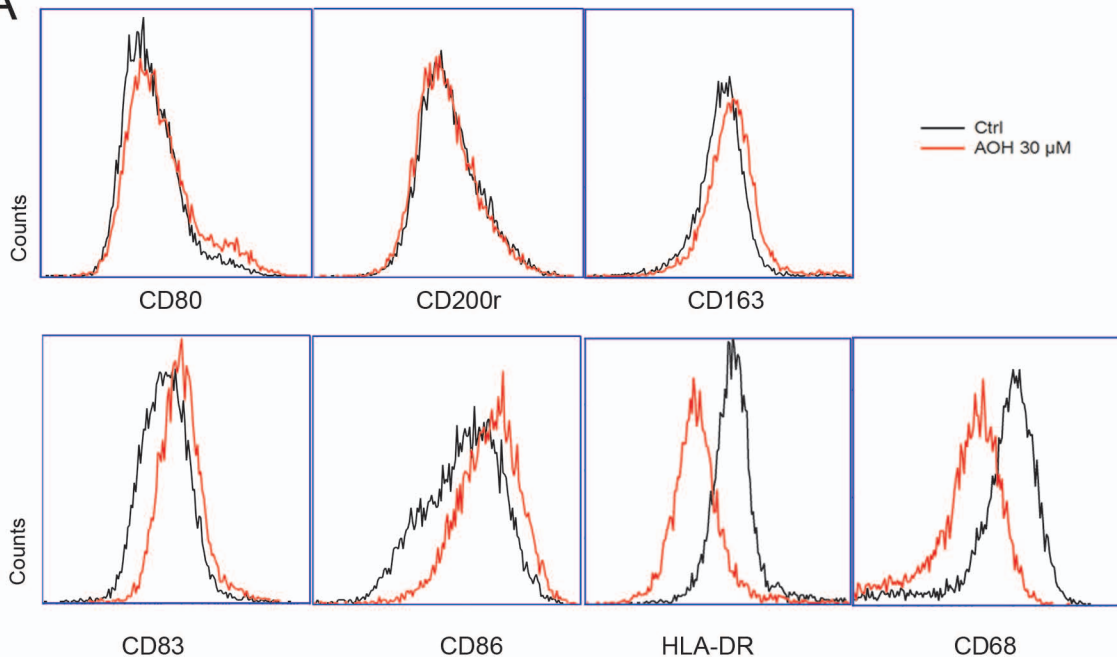


Fig 6, 2-column

**A**



**B**

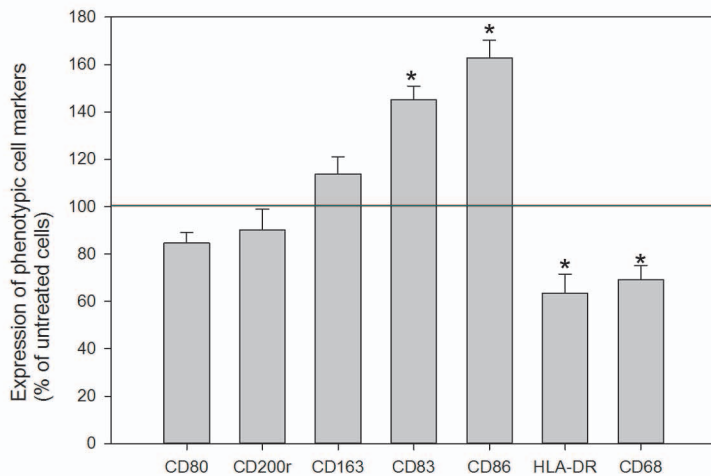


Fig 7, single column

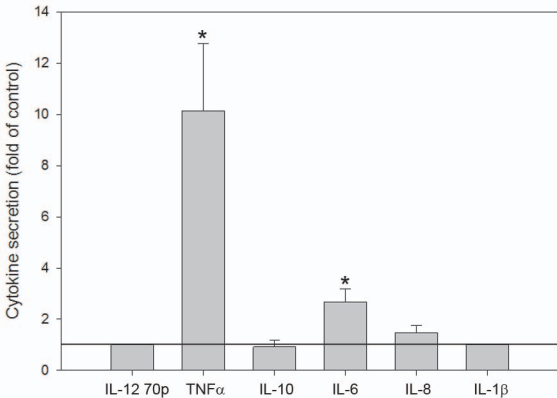
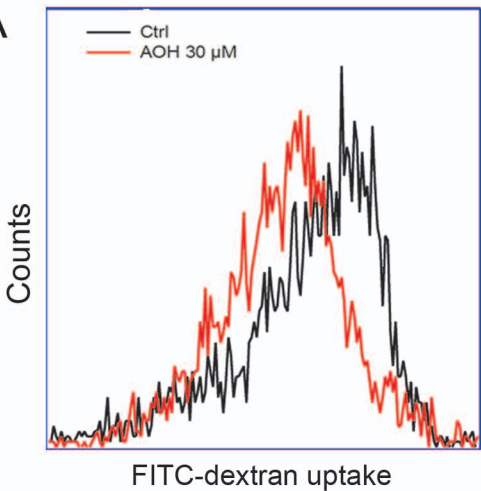
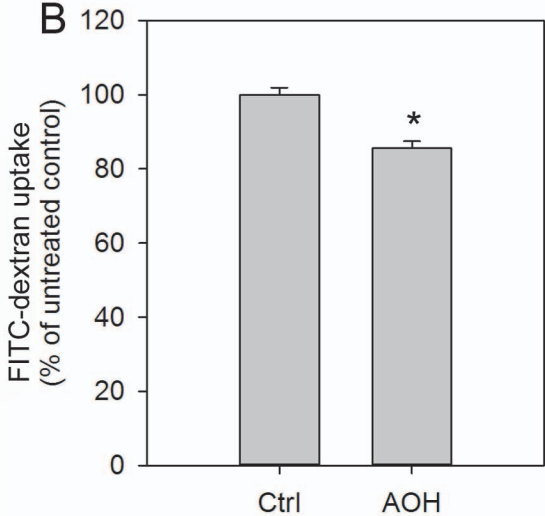


Fig 8, single column

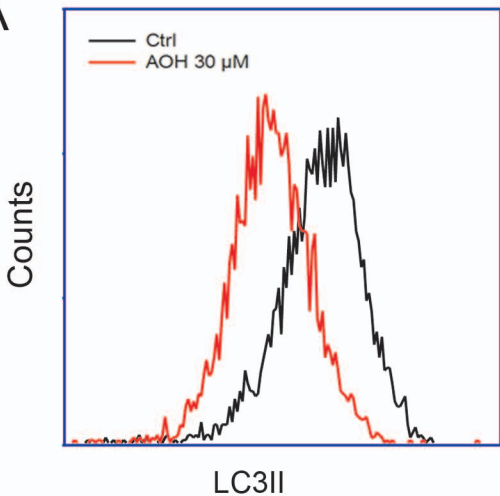
**A**



**B**



**A**



**B**

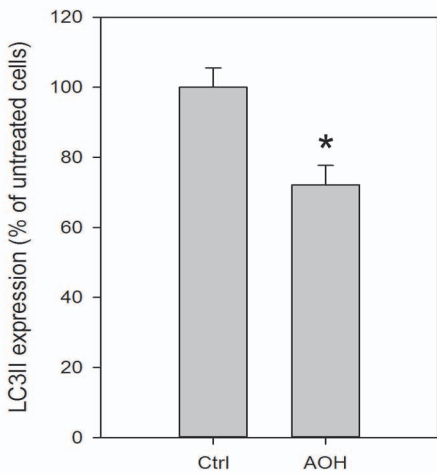
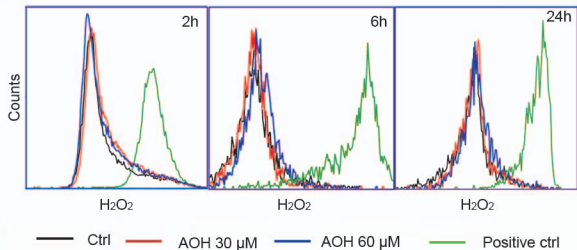


Fig 10, single column

A



B

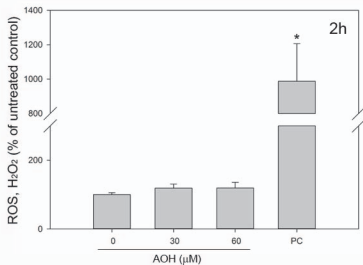


Fig 11, 2-column

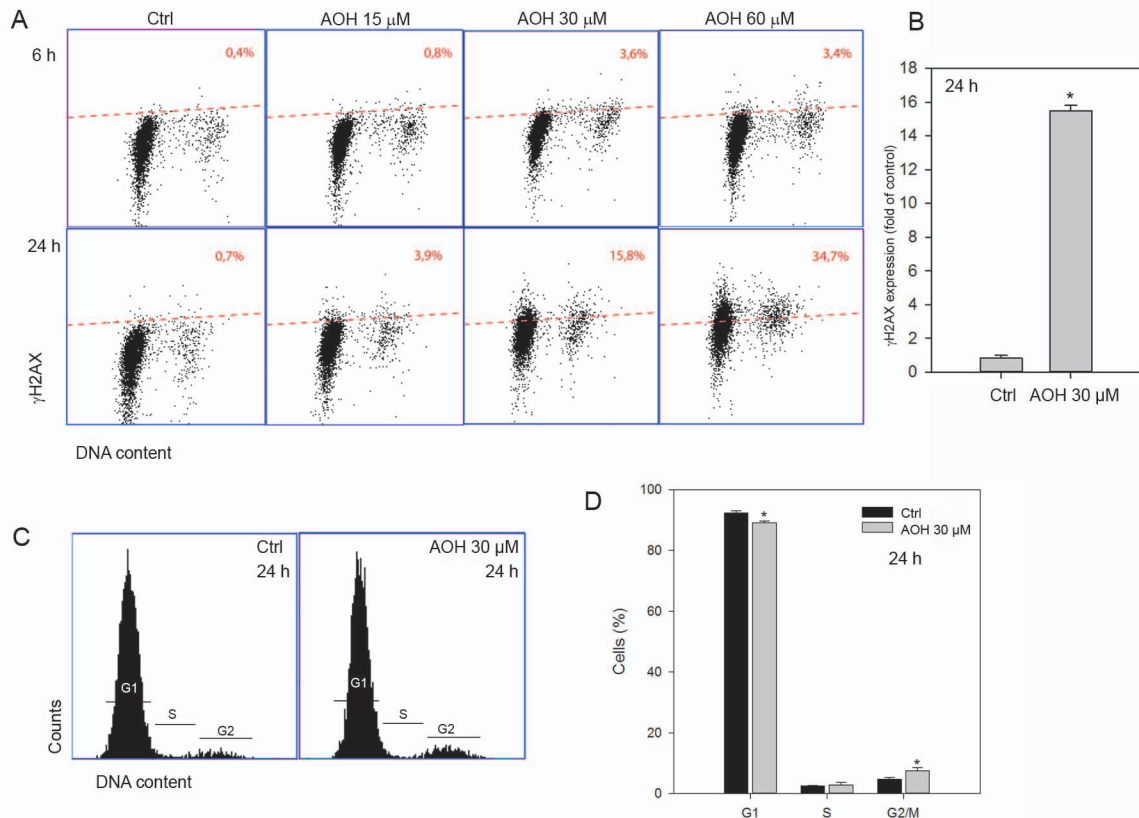


Fig S1, supplementary, single column

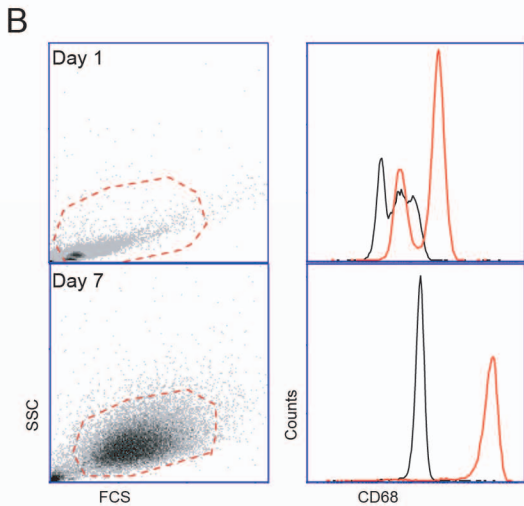
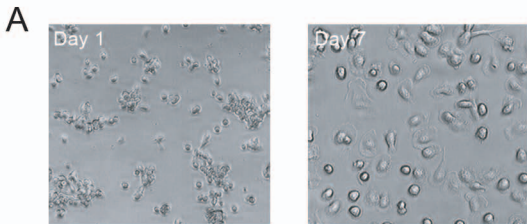


Fig S2, supplementary, single column

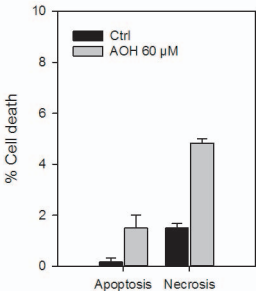
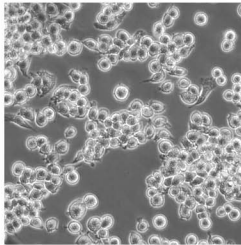
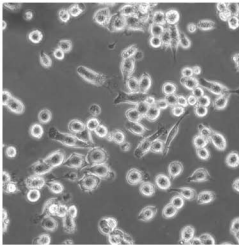


Fig.S3, Supplementary, single column

Ctrl



AOH



AOH+NAC

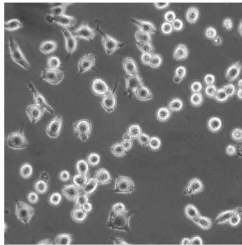
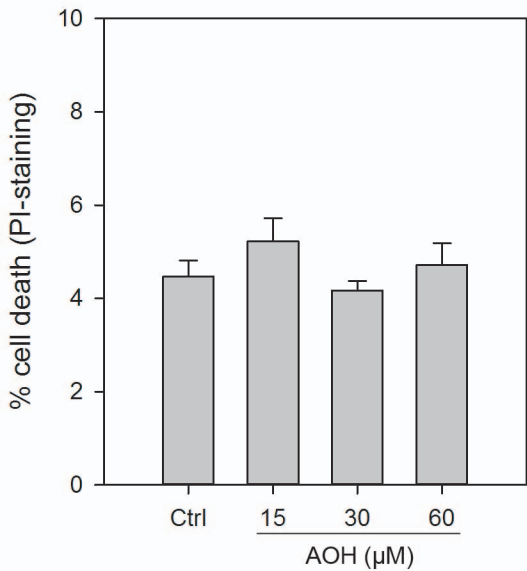
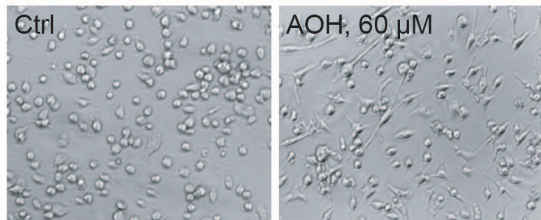


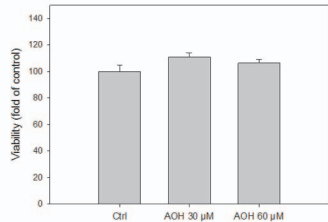
Fig S4, supplementary. single column



A



B



C

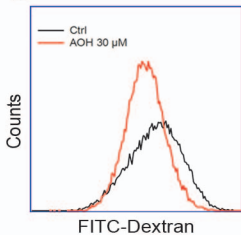
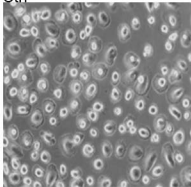
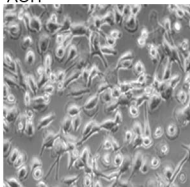


Fig S6, Supplementary, single column

Ctrl



AOH



AOH + NAC

